Journal of Testing and Evaluation, Vol. 38, No. 2
Paper ID JTE102261
Available online at: www.astm.org

Diego Ferreño,[1] *Isidro A. Carrascal,*[2] *Sergio Cicero,*[3] *and E. Meng*[4]

Characterization of Mechanical Properties of a Shock Absorber Polyurethane Foam for Elevators. Numerical Fitting of Mechanical Behavior Models for Hyperelastic and Elastomeric Foam Materials

ABSTRACT: The elastic cellular polyurethane elastomer is widely used to manufacture shock absorbers for elevators, due to its excellent conditions for absorption of energy and vibration damping. In this paper, a complete mechanical characterization of this material was performed including the uniaxial compressive test, the planar test, and the volumetric and the simple shear test. From the experimental results, several models of behavior for hyperelastic and elastomeric foam materials have been analyzed by fitting their corresponding material parameters. The scope of this work includes the Ogden model, the Van der Waals model, and polynomial and elastomeric foam forms.

KEYWORDS: cellular polyurethane elastomer, mechanical characterisation, Ogden, Van der Waals, polynomial, elastomeric foam, ABAQUS

Introduction

In today's world, an elevator is understood as a vehicle for vertical transport of persons and/or materials. The vehicle must include the elements which are necessary to minimize the consequences in case of a sudden breakage of the hoisting cable. Since 1853, when Elisha Graves Otis incorporated an elevator brake to the platform as one of the safety devices, to our days, elevators have evolved in every aspect and, in particular, in the field of safety; as a consequence of this development, skyscrapers became a practical reality.

Today, several complementary safety systems (like governors, electromagnetic brakes, and load sensors) are included in any elevator. Shock absorbers are one of these indispensable safety devices, consisting of elements placed in the bottom of the shaft which work as a deformable limit for the travel of the cab and of the counterweight. Spring and hydraulic shock absorbers are widely used in the market; nevertheless, another kind of absorbers, known as buffers, have recently appeared, offering certain specific advantages, such as:

(1) Wider range of loads;
(2) Inexpensive solution;
(3) Easy to handle due to its small volume and weight;
(4) Able to provide a softer elevator cab landing, as they are very highly deformable; and
(5) High capacity for cushioning of oscillations.

The standard UNE-EN 81 [1–3], currently in force in Europe, classifies buffers into the category of "energy accumulative shock absorbers." According to UNE-EN 81 [1–3] these elements must fulfill several demanding requirements when stopping an elevator.

Manuscript received December 5, 2008; accepted for publication October 24, 2009; published online December 2009.

[1]Laboratorio de la División de Ciencia e Ingeniería de los Materiales (LADICIM), E.T.S. de Ingenieros de Caminos, Canales y Puertos, Universidad de Cantabria, Av. Los Castros, s/n. 39005 Santander, Spain (Corresponding author).

[2]Laboratorio de la División de Ciencia e Ingeniería de los Materiales (LADICIM), E.T.S. de Ingenieros de Caminos, Canales y Puertos, Universidad de Cantabria, Av. Los Castros, s/n. 39005 Santander, Spain.carrasci@unican.es

[3]Laboratorio de la División de Ciencia e Ingeniería de los Materiales (LADICIM), E.T.S. de Ingenieros de Caminos, Canales y Puertos, Universidad de Cantabria, Av. Los Castros, s/n. 39005 Santander, Spain ciceros@unican.es

[4]Ascensores Amuesa Polígono Industrial Raos, Parcela 13H, Maliaño, 39600 Santander, Spain.lacaller@unican.es

Aims of the Present Work

A detailed study of the mechanical behavior of a buffer shock absorber has been developed. In Fig. 1 a scheme of the component can

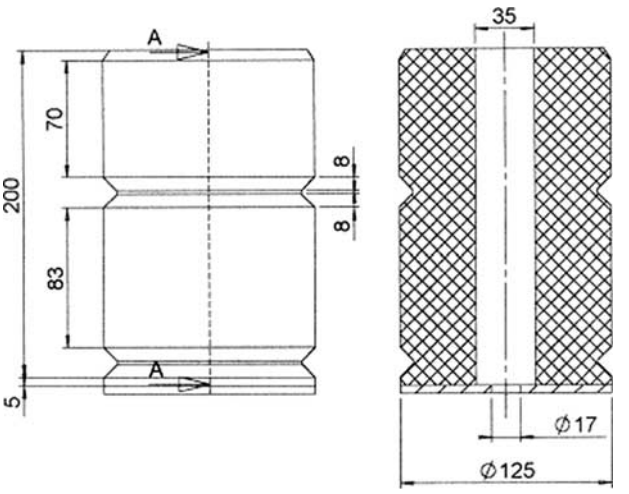

FIG. 1—*Scheme of the buffer shock absorber including its geometrical dimensions.*

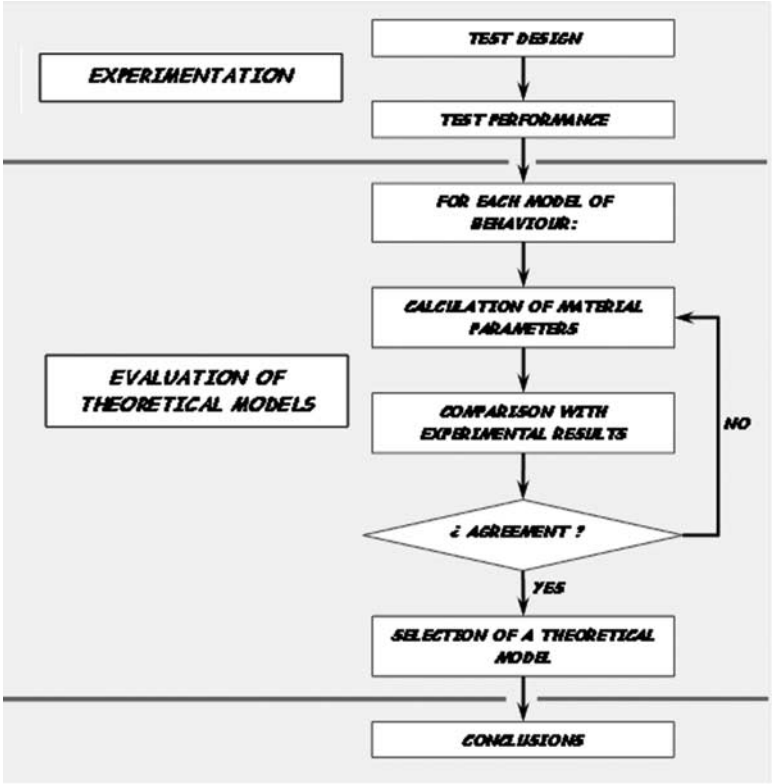

FIG. 2—*Flowchart of the work developed.*

be seen including the relevant geometrical dimensions. It has been manufactured in an isotropic elastomeric material, with deeply nonlinear mechanical behavior.

The mechanical response of this kind of materials is usually very complex. Nevertheless, theoretical models to describe the behavior of nonlinear elastomeric materials can be found in the literature. In this work, the most relevant models have been evaluated by fitting their material parameters from the experimental information, thus selecting the most representative one. The usefulness of this result is evident: After selecting a model and obtaining its parameters, the behavior of the material is perfectly known and, for example, the conditions imposed by UNE-EN 81 [1–3] can be checked by means of a finite elements model.

The sequence of actions followed is here summarized. The flowchart in Fig. 2 outlines the activities here developed.

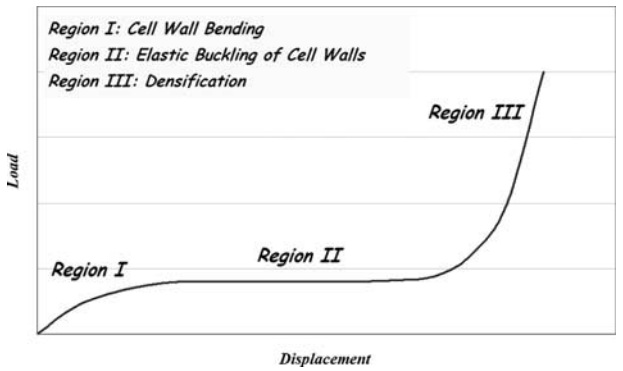

FIG. 3—*Typical appearance of a load-displacement curve in a compressive test on an elastic material.*

(1) The mechanical response of the material has been determined through several different tests performed on specimens of small dimensions extracted from one of the available buffers;
(2) The experimental results have been incorporated in the main theoretical models considered in the literature to describe the mechanical behavior of elastomers, by fitting their corresponding parameters; and
(3) Among the theoretical models analyzed, the one which best describes the material here studied has been selected.

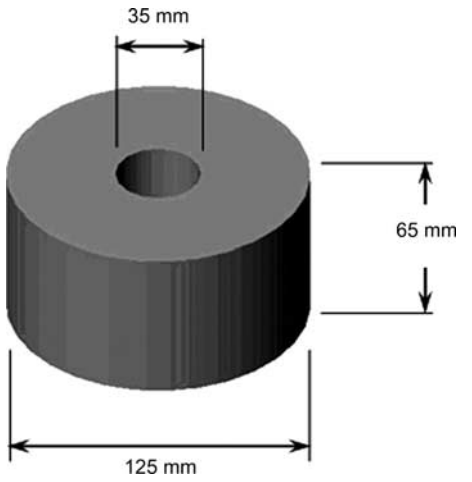

FIG. 4—*Isometric perspective of the compressive test specimen including geometrical dimensions.*

FIG. 5—*Photograph of the test device, including the LVDT used to measure transversal displacements during compression.*

Material

The buffer shock absorber, the object of the study in this work, is made of a highly elastic cellular polyurethane (PU) elastomer with a density close to 400 kg/m^3. PU is a polymer with highly versatile properties and a wide range of commercial applications that presents a structure of open and closed cells which are responsible for its exceptional mechanical properties. The main characteristics of the material are summarized in the following and, as can be appreciated, they are coherent with the desirable properties for a buffer shock absorber, as stated in the Introduction:

(1) Great loading capacity;
(2) Compression strains up to 80 % even under dynamic conditions;
(3) High energy absorption;
(4) High volume compressibility, which is responsible for their relatively low transverse expansion during load application;
(5) Very good vibration damping;
(6) Dimensional stability;
(7) Wear and tear resistant;
(8) Temperature range from −30 to +80 °C; and
(9) Good resistance against mineral oils, grease, petrol, and against ageing.

The PU buffer was manufactured by reaction injection molding (RIM) [4]. It is produced by the chemical reaction of isocyanate and polyhydric alcohol. RIM involves the injection of liquid PU systems into a mold. The components then polymerize within the mold. Typically, this low temperature process takes less than a minute to complete, including time for mixing, curing, and demolding. During the process, gas cells are generated, thus providing the component with excellent cushioning properties.

To the present time, the cellular structure of PU foam and its effect on the mechanical response of the material has been studied by several authors [5–8]. In addition, the thermal and compression behavior of PU material manufactured for roof insulation was investigated in detail in Ref 9.

Considerations about the Mechanical Behavior of the Material

The main mechanical characteristic that defines an elastomer is the ability to withstand great elastic elongations, recoverable after unload. Most of the elastomers show small compressibility and are, in general, known as hyperelastic materials. On the other hand, among the rubberlike materials, the elastomeric foams can be distinguished because they manifest a highly compressible character. In both cases, since the long molecular chains are randomly oriented, the material is initially isotropic.

Figure 3 shows the typical appearance of the load-displacement curve of elastomeric foam under compression. Three different regions can be distinguished [10], which are a consequence of the cellular structure in the material:

(1) For small strains, less than 5 % (Region I), the walls of the cells slowly bend and the foam deforms in a linear elastic manner;
(2) In the second stage (Region II), a plateau is reached as a

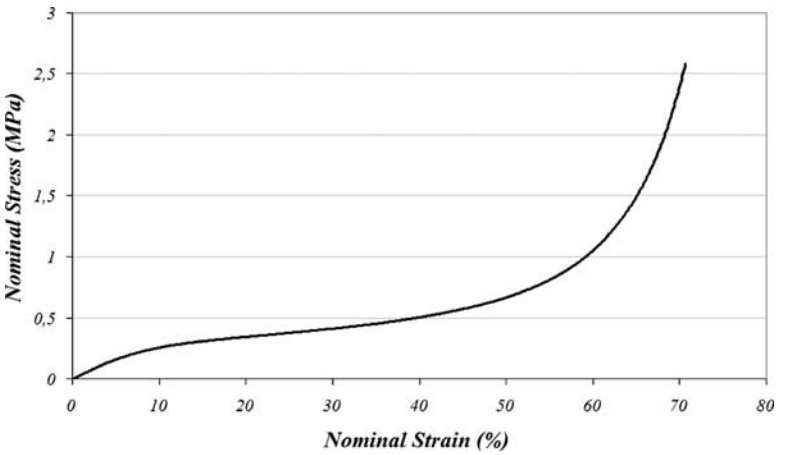

FIG. 6—*Nominal stress versus nominal strain curve for the uniaxial quasi-static compressive test.*

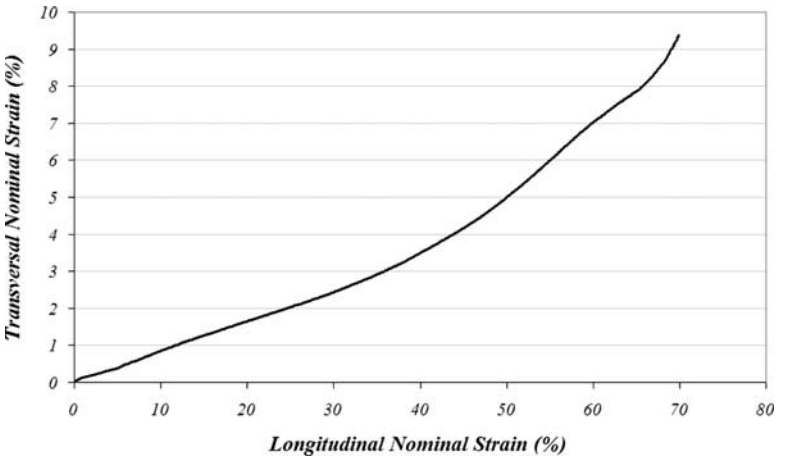

FIG. 7—*Experimental curve relating transversal and longitudinal nominal strains.*

consequence of the collapse in the cells (elastic buckling) that compresses the gas inside; and

(3) In the last stage, a densification of the material occurs: After the collapse of the cells, they are completely compressed and hence the material experiences important stiffening (great load increase for small displacements).

From another perspective [11], hyperelastic (or Green-elastic) materials are those for which a strain-energy (per unit of undeformed volume) potential function exists, being a scalar function of the strain tensor components, $U = U(E_{ij})$. The components T_{ij} of the stress tensor can be expressed according to Eq 1

$$T_{ij} = \frac{\partial U(E)}{\partial E_{ij}} \tag{1}$$

This definition is independent of the compressibility of the material, thus including the two possibilities described earlier (namely, hyperplasic or elastomeric foams). The bibliography [12] provides several expressions for the strain energy potential, U. In the case of isotropic materials, the models can be expressed in terms of the strain invariants (together with material parameters to be fitted from experimental information). In most cases, the strain energy potential forms are written as separable functions of a deviatoric component and a volumetric component, as in expression 2

$$U = U_{\text{dev}}(\bar{I}_1, \bar{I}_2) + U_{\text{vol}}(J^{\text{el}}) \tag{2}$$

Some notations will now be introduced. In the latter expression 2, $\bar{I}_1$ and $\bar{I}_2$ represent, respectively, the first and second deviatoric strain invariants defined as follows:

$$\bar{I}_1 = \bar{\lambda}_1^2 + \bar{\lambda}_2^2 + \bar{\lambda}_3^2 \tag{3}$$

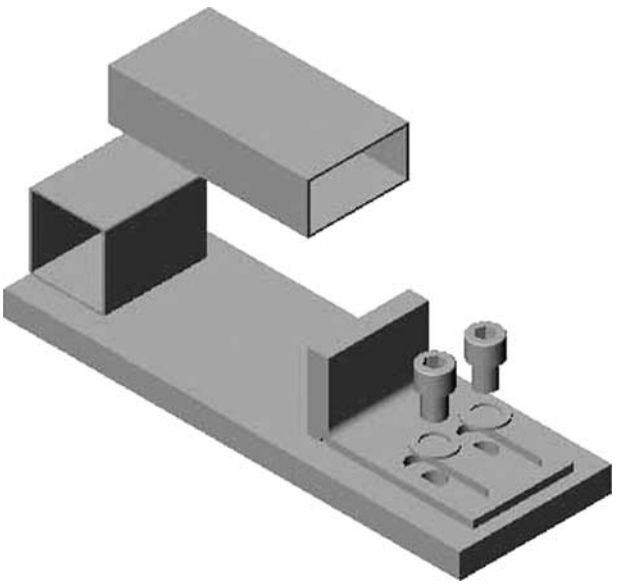

FIG. 8—*Experimental arrangement used to perform the planar test.*

FIG. 9—*Photograph of the experimental arrangement for the planar test.*

$$\bar{I}_2 = \bar{\lambda}_1^{(-2)} + \bar{\lambda}_2^{(-2)} + \bar{\lambda}_3^{(-2)} \tag{4}$$

where:

$\bar{\lambda}_i$=deviatoric stretches (Eq 5)

$$\bar{\lambda}_i = J^{-1/3}\lambda_i \tag{5}$$

Expression 5 shows the relation between the deviatoric stretches, $\bar{\lambda}_i$, and the principal stretches, λ_i, J being the total volume ratio which accounts for the compressibility of the material; this is defined as $J=\det(F)$ where the deformation gradient, F, expressed in the principal directions of stretch is given in Eq 6

$$F = \begin{bmatrix} \lambda_1 & 0 & 0 \\ 0 & \lambda_2 & 0 \\ 0 & 0 & \lambda_3 \end{bmatrix} \tag{6}$$

When $J=1$ (and therefore, $\lambda_1\lambda_2\lambda_3=1$) the material is incompressible. Finally, in Eq 2 J^{el} represents the elastic volume ratio, given by Eq 7

$$J^{el} = \frac{J}{J^{th}} \tag{7}$$

where:

$J^{th}=(1+\varepsilon^{th})^3$, and

ε^{th}=linear thermal expansion strain (not relevant for the conditions of constant temperature).

Each model includes a set of material parameters which are, in principle, unknown. They can be evaluated from empirical results coming from mechanical characterisation tests. The finite elements software ABAQUS [12] is provided with a set of theoretical models with the shape Eq 2 and includes the tools to evaluate the models from the tests, thus fitting their parameters. The material constants are determined through a least-squares-fit procedure which minimizes the relative error (RE) in stress. For the n nominal-stress-nominal-strain data pairs, the relative measure RE, given in Eq 8, is minimized

$$\mathrm{RE} = \sum_{i=1}^{n} \left(1 - \frac{T_i^{th}}{T_i^{test}}\right)^2 \tag{8}$$

T_i^{test} being a stress value from the stress data, and T_i^{th} the value coming from the nominal stress expression evaluated. ABAQUS [12] minimizes the RE rather than an absolute error measure since this provides a better fit at lower strains.

ABAQUS distinguishes between hyperelastic materials (see "Hyperelastic Materials") and elastomeric foams (see "Elastomeric Foam Model"), following the distinction presented earlier based on the compressibility of the material. Next, the models analyzed in this work are briefly presented.

Hyperelastic Materials

Several different sets of hyperelastic forms are available in Ref 12, namely, the Ogden (see "Ogden Form"), Van der Waals (see "Van der Waals Form"), and several polynomial models (see "Polynomial Models").

Ogden Form—This is defined according to expression 9 for the strain energy potential

$$U = \sum_{i=1}^{N} \frac{2\mu_i}{\alpha_i^2}(\bar{\lambda}_1^{\alpha_i} + \bar{\lambda}_2^{\alpha_i} + \bar{\lambda}_3^{\alpha_i} - 3) + \sum_{i=1}^{N} \frac{1}{D_i}(J^{el} - 1)^{2i} \tag{9}$$

N, μ_i, α_i, and D_i are material parameters (the last three temperature dependant). The first one, N, must be chosen *a priori* by the user.

Van der Waals Form—This form is represented in expression 10 where the definitions 11 and 12 must be considered.

$$U = \mu\left\{-(\lambda_m^2 - 3)[\ln(1-\eta) + \eta] - \frac{2}{3}a\left(\frac{\bar{I}-3}{2}\right)^{3/2}\right\} + \frac{1}{D}\left(\frac{J_{el}^2 - 1}{2} - \ln J_{el}\right) \tag{10}$$

$$\bar{I} = (1-\beta)\bar{I}_1 + \beta\bar{I}_2 \tag{11}$$

$$\eta = \sqrt{\frac{\bar{I}-3}{\lambda_m^2 - 3}} \tag{12}$$

Polynomial Models—The general form of the strain energy potential according to a polynomial model is given by Eq 13

$$U = \sum_{i+j=1}^{N} C_{ij}(\bar{I}_1 - 3)^i(\bar{I}_2 - 3)^j + \sum_{i=1}^{N} \frac{1}{D_i}(J^{el} - 1)^{2i} \tag{13}$$

where N, C_{ij}, and D_i being material parameters (the last two, temperature dependant). The first one, N, must be chosen a priori by the user. Several particular cases of polynomial models can be distinguished, the most relevant being the Money—Rivlin and reduced polynomial forms. These have not been taken into account for this work, as only the general expression 13 has been considered.

Elastomeric Foam Model

When a strong influence of the cellular structure in the material is to be expected, leading to important compressibility, models of the kind (Eq 14) must be employed

$$U = \sum_{i=1}^{N} \frac{2\mu_i}{\alpha_i^2}\left[\hat{\lambda}_1^{\alpha_i} + \hat{\lambda}_2^{\alpha_i} + \hat{\lambda}_3^{\alpha_i} - 3 + \frac{1}{\beta_i}((J^{el})^{-\alpha_i\beta_i} - 1)\right] \tag{14}$$

where:

N, μ_i, α_i, and β_i=material parameters (the last three, temperature dependant) to be fitted through the least-squares-fit procedure mentioned earlier.

N must be chosen a priori by the user.

Experimental Part

To characterize the material of the shock absorber, different specimen geometries have been machined from one of the buffers available depending on the test to be developed. The tests performed are the uniaxial compressive test, which represents the normal operative conditions of the buffer (see "Uniaxial Quasi-Static Compression Test"), the planar test (see "Planar Test"), the volumetric test (see "Volumetric Test (Triaxial)"), and the simple shear test (see "Simple Shear Test"). Except for the volumetric one, which requires a more sophisticated experimental device, the rest of the me-

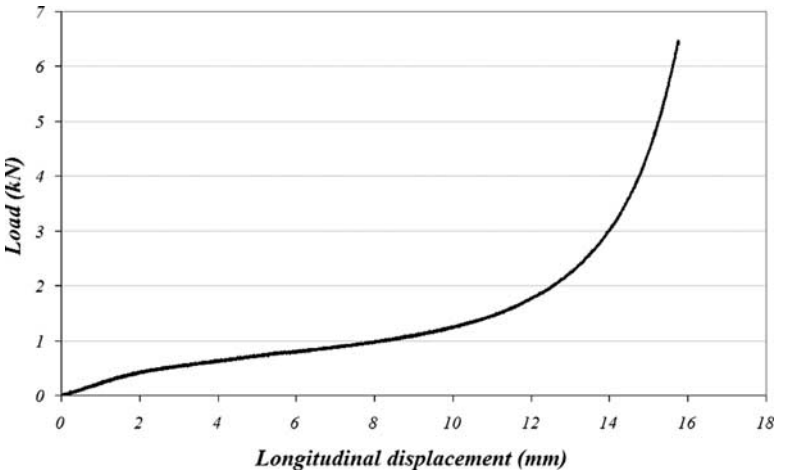

FIG. 10—*Experimental curve showing nominal stress against nominal strain.*

chanical tests have been performed in a universal INSTRON 8501 hydraulic machine (able to work also under static or dynamic conditions) with a load capacity of 100 kN.

For the machining of specimens and devices and for the test performances, the recommendations given in standard UNE-ISO 23529 [13] have been followed. During the cutting process of the specimens, no lubricants have been used (in order to keep the specimen clean) and, to avoid the excessive heating of the piece, the cutting speed was kept low. The steel blade has been previously sharpened to avoid the appearance of defective surfaces. Thanks to these precautions, a very accurate surface finishing has been achieved in all cases.

Uniaxial Quasi-Static Compression Test

The uniaxial deformation mode is characterized in terms of the principal stretches, λ_i, as Eq 15, where λ_U is the stretch in the loading direction

$$\lambda_1 = \lambda_U; \quad \lambda_2 = \lambda_3 \tag{15}$$

When an incompressible material is being tested, $\lambda_2 = \lambda_3 = (\lambda_U)^{-1/2}$.

Figure 4 shows an isometric projection including the geometrical dimensions of the specimen machined from one of the available buffers for the uniaxial compressive test. To obtain a uniform resistant section in the specimen, this was taken from the region of the buffer between the two circumferential notches (see Fig. 1). According to the dimensions in Fig. 4 (also in Fig. 1), the nominal section of the specimen is $A_0 = 11\,310$ mm^2 and the nominal length, $L_0 = 65$ mm. This information is of relevance as nominal-stress and nominal-strain values must be supplied to ABAQUS for the fitting of parameters.

The experimental conditions consist in a displacement control test, under quasi-static regime (at a rate of 0.1 mm/s). The photograph of the test device presented in Fig. 5 allows the buffer specimen to be distinguished together with the steel plates used to apply the relative displacement between its upper and lower faces. The linear variable differential transformer (LVDT) attached to record the transversal displacements during the test can also be appreciated in Fig. 5. It should be pointed out that, to minimize the barrel formation, frictionless test conditions have been provided by means of a thin lubricant layer on each face of the specimen.

The experimental nominal-stress versus nominal strain curve can be appreciated in Fig. 6. Also Fig. 7 shows the curve relating transversal and longitudinal nominal strains. The initial Poisson ratio, ν_0, can be calculated by linear fitting of the initial part of the curve in Fig. 7 to obtain the result Eq 16 with the correlation coef-

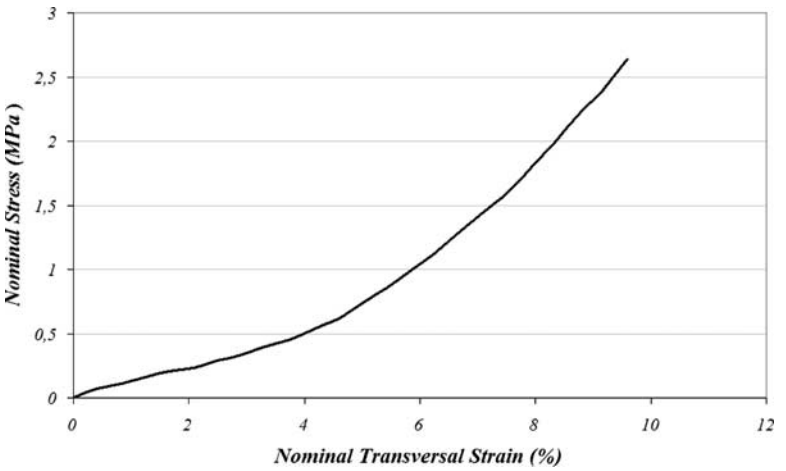

FIG. 11—*Experimental curve relating the Nominal Stress with the nominal transversal strain.*

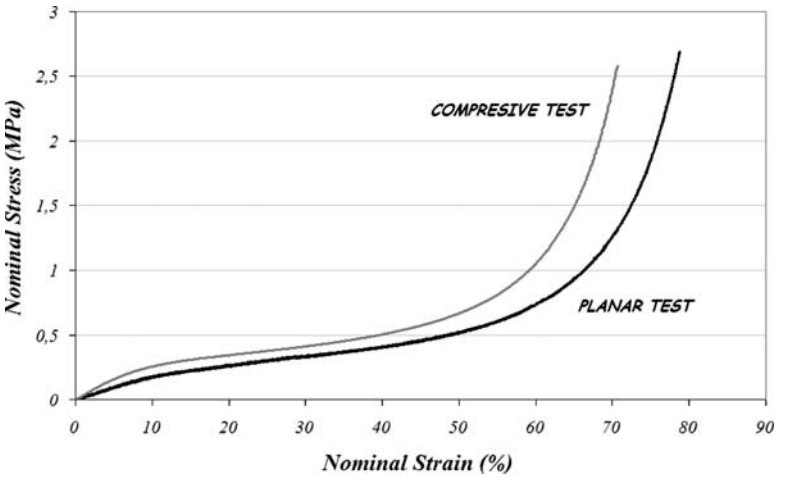

FIG. 12—*Comparison between the mechanical response in compression test and planar test.*

ficient Eq 17. As can be observed, the linear relation between longitudinal and transversal strains is lost for longitudinal nominal strains over 30–35 %

$$\nu_0 = 0.082 \tag{16}$$

$$R^2 = 0.9988 \tag{17}$$

Planar Test

The planar deformation mode is characterized in terms of the principal stretches, λ_i, as Eq 18, where λ_S is the stretch in the loading direction

$$\lambda_1 = \lambda_S; \quad \lambda_2 = 1 \tag{18}$$

When an incompressible material is being tested, $\lambda_3 = (\lambda_S)^{-1}$.

To approximate the deformation mode (Eq 18), the experimental arrangement shown in Fig. 8 has been designed and fabricated. Planar tests are usually done with a thin, short, and wide rectangular strip of material (in this case, thickness: 20 mm; width: 30 mm; length: 80 mm, respectively) fixed on its wide edges to rigid loading clamps. The comparatively long size of the specimen in the length direction and the rigid clamps allow using the approximation $\lambda_2 = 1$; here, the specimen was placed in the device shown in Fig. 8 which perfectly fits the ends of the specimen in the longer dimension, that is, there is no deformation in the wide direction of the specimen.

In Fig. 9, a photograph of the test can be appreciated. As in the compression test, an LVDT has been attached to record the transversal displacements during the planar test. Also, to minimize the barrel formation, lubricant layers have been used on each side of the specimen.

The results of the planar test are shown in Fig. 10 (nominal stress versus nominal strain) and Fig. 11, respectively (nominal stress versus nominal transversal strain). The differences between the mechanical response of the material under compression (see "Uniaxial Quasi-Static Compression Test") and planar conditions are evident in Fig. 12, where the respective experimental curves are compared.

Volumetric Test (Triaxial)

The volumetric deformation mode consists of all principal stretches being equal

$$\lambda_1 = \lambda_2 = \lambda_3 = \lambda_V \tag{19}$$

The volumetric test allows the compressibility of the material to be evaluated. The experimental process consists of applying an increasing hydrostatic stress state to the specimen recording simultaneously its volume variation.

It should be pointed out that this kind of characterisation is seldom performed on structural materials; for this reason it was necessary to adapt the geotechnical triaxial test, widely used in the characterisation of soils, to the rubberlike material here analyzed. The recommendations presented in the standard UNE 103402 [14] have been followed.

In the conventional triaxial test, a cylindrical specimen of soil (of PU, in this case), previously saturated in water then encased in a (impermeable) rubber membrane, is placed in a triaxial compression chamber, subjected to a confining fluid pressure, and then loaded axially to failure. In this case, for the goal here pursued of measuring the compressibility, during the first stage, the fluid pressure is monotically increased, the last stage of axial loading not being necessary. Here a cylindrical specimen (machined from the buffer) was used its geometrical dimensions being: Height—70 mm; diameter—35 mm.

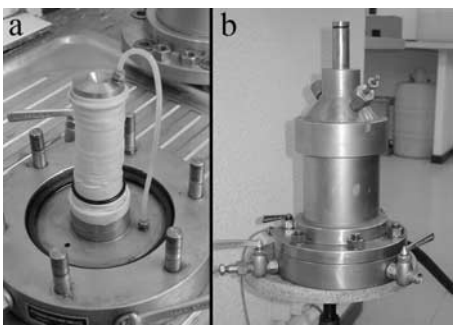

FIG. 13—*Photograph of the specimen covered with the membrane (left) and triaxial chamber (right).*

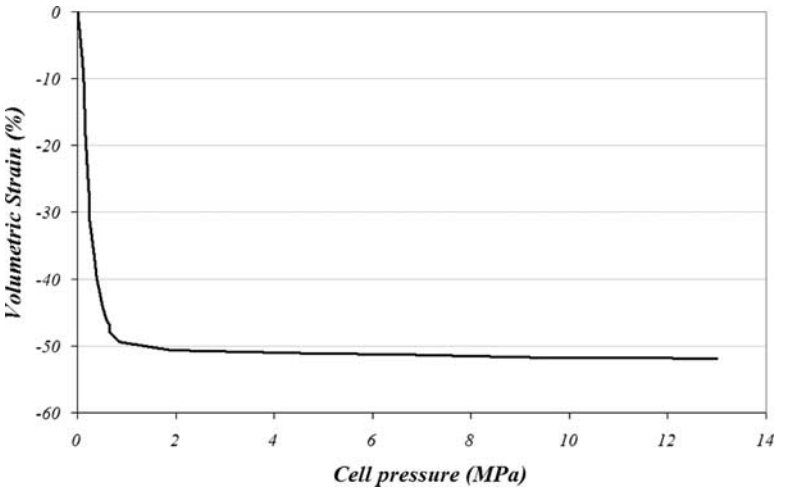

FIG. 14—*Volumetric strain in the specimen graphed as a function of cell pressure.*

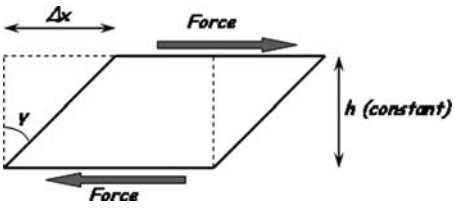

FIG. 15—*Scheme of the simple shear deformation.*

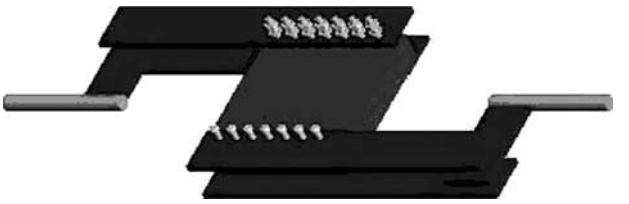

FIG. 16—*Experimental arrangement used in the simple shear test.*

At the ends of the specimen, two porous plates (whose porosity is between 10^{-3} and 10^{-4} m/s) are placed, with connections that permit controlled drainage of pore water from the specimen, thus allowing the volume variation to be measured. The test is called "triaxial" because the three principal stresses are assumed to be known and controlled. In obtaining the compressibility of the elastomeric material, the three principal stresses are equal to the chamber fluid pressure (hydrostatic stress state). Figure 13 (left) shows a photograph of the membrane covering the specimen together with the porous plates, and the drainage connections. The right part of the photograph presents the triaxial chamber used for the test.

Prior to saturating the specimen, the (dry) density of the material was measured obtaining a result of 390 kg/m^3, as expected (see "Material"); the open porosity of the material could be calculated taking into consideration the amount of water necessary for saturation, yielding a result of 52.1 %. Finally, after performing the test, the curve relating the volumetric strain (i.e., change in volume per unit of original volume) with the cell pressure was obtained, as shown in Fig. 14.

Simple Shear Test

Simple shear is described by the deformation gradient Eq 20 where γ is the shear strain

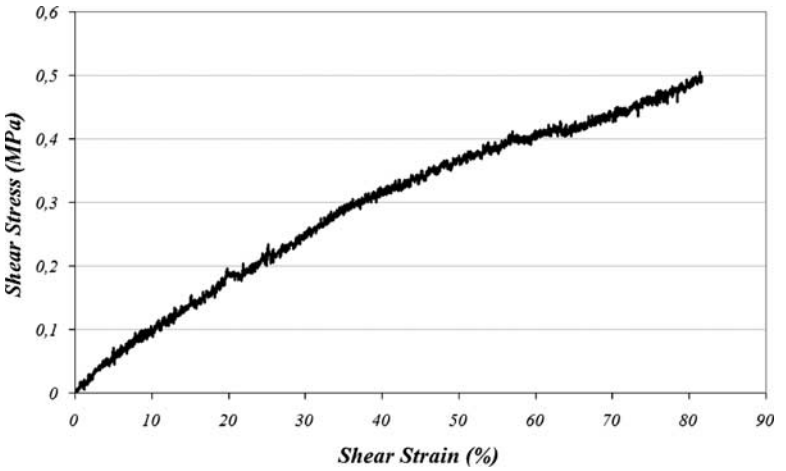

FIG. 18—*Experimental curve for shear test showing shear stress versus shear strain.*

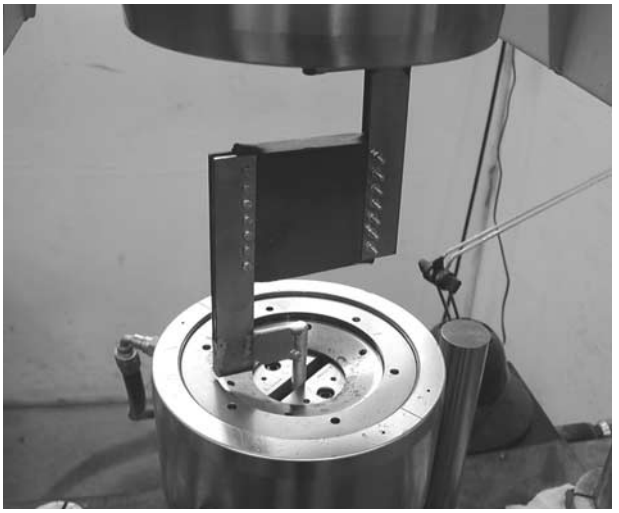

FIG. 17—*Photograph of the specimen during shear test.*

TABLE 1—*Fitting parameters and RMSE, Ogden form, N*=1.

μ_1	0.117938
α_1	−0.273514
D_1	1.02069
RMSE (%)	52.88

TABLE 2—*Fitting parameters and RMSE, Ogden form, N*=3.

	i=1	i=2	i=3
μ_i	−57.57	26.74	31.03
α_i	1.924	2.03	1.814
D_i	0.5745	−0.05783	0.01962
RMSE (%)	39.16		

TABLE 3—*Fitting parameters and RMSE, Van der Waals form.*

μ	0.255193
λ_m	7.73877
a	0.730524
β	0
D	2.13921
RMSE (%)	46.34

TABLE 4—*Fitting parameters and RMSE, polynomial form.*

D_1	1.021
C_{10}	−0.02996
C_{01}	0.0469
RMSE (%)	49.25

TABLE 5—*Fitting parameters and RMSE, elastomeric foam form.*

	i=1	i=2	i=3
μ_i	−6.488	7.37	−0.1436
α_i	3.121	3.423	9.816
β_i	0.1874	0.1765	0.5758
RMSE (%)	25.94		

$$F=\begin{bmatrix}1 & \gamma & 0\\ 0 & 1 & 0\\ 0 & 0 & 1\end{bmatrix} \tag{20}$$

For this deformation $J=\det(F)=1$. A schematic demonstration of simple shear deformation is shown in Fig. 15. As can be appreciated, $\gamma=\Delta x/h$.

The experimental arrangement designed to perform the shear test can be seen in Fig. 16. It was necessary to incorporate this device in order to convert the uniaxial force applied by the INSTRON 8501 machine into a shear pair of (eccentric) forces. The dimensions of the specimen (machined from one of the available buffers) are length of 82 mm, width of 80 mm, and thickness of 16 mm. In Fig. 17, a photograph of the specimen being tested can be appreciated. The experimental results are presented in Fig. 18 where the shear stress is plotted against the shear strain, γ.

Evaluation of Theoretical Material Models

In "Considerations about the Mechanical Behavior of the Material," a brief description of several models representing the mechanical response of hyperelastic materials and elastomeric foams was presented. The empirical results obtained from specimens extracted from one of the available buffers (see "Experimental Part") allow the parameters included in the different functions for the strain energy potential to be evaluated. ABAQUS is provided with numerical tools (property module) to perform the fitting of parameters by means of a least-squares-fit procedure from the experimental curves presented in "Experimental Part." For all tests, the strain data, including the lateral strain data, should be given as nominal strain values (change in length per unit of original length) and stress data as nominal stress values (force per unit of cross-sectional area).

Once the parameters have been obtained for each material model, two different ways to check the reliability of the solution are available. On the one hand, after the calculations have been performed, the root mean square error (RMSE) is available from the software. It should be pointed out that RMSE has the disadvantage of being an estimator that heavily weights outliers; therefore, RMSE represents a nonrobust estimator. This is a result of the squaring of each term, which effectively weights large differences between the model and the experimental data more heavily than small ones. Although particular values of RMSE other than zero are meaningless in and of themselves, they may be used for comparative purposes. Two or more statistical models may be compared using their RMSEs as a measure of how well they explain a given set of observations: The unbiased model with the smallest RMSE is generally interpreted as best explaining the variability in the observations.

On the other hand, it is possible to plot, for the different tests, the curves that correspond to these model material and fitting parameters. This allows a comparison between the real behavior (i.e., the

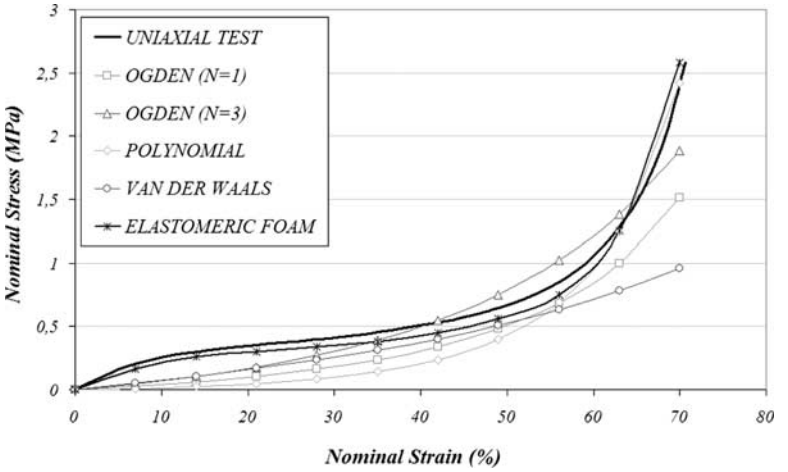

FIG. 19—*Comparison between experiments and theoretical models for uniaxial compressive test.*

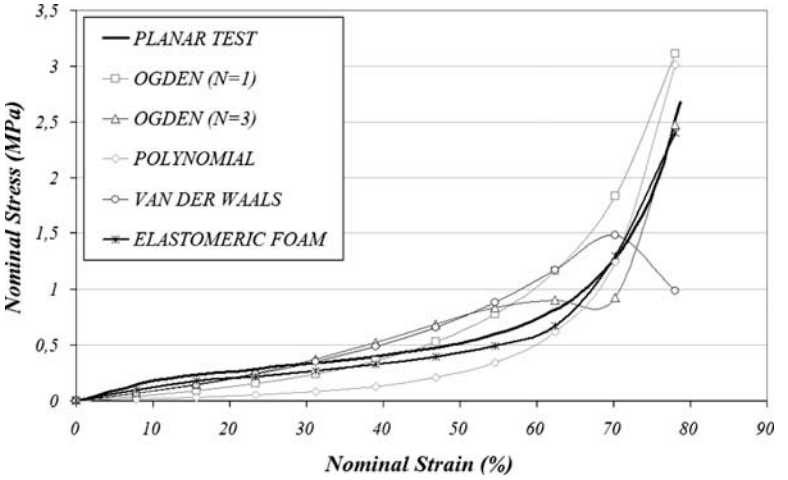

FIG. 20—*Comparison between experiments and theoretical models for planar test.*

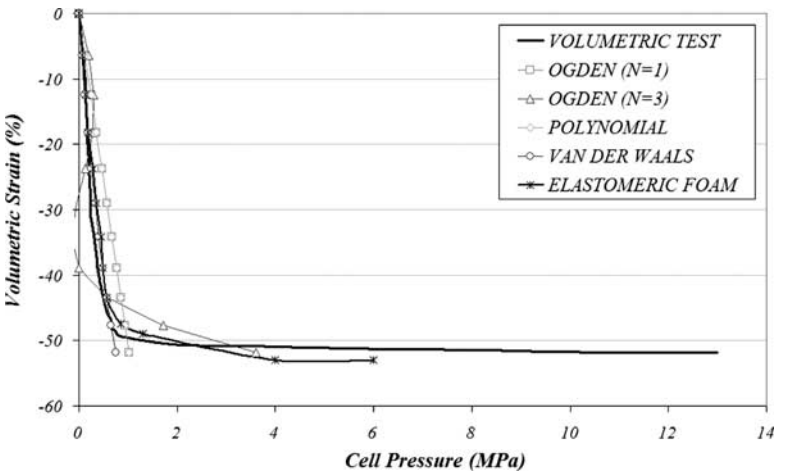

FIG. 21—*Comparison between experiments and theoretical models for volumetric test.*

experimental results) with the response of the theoretical material to be directly visualized.

As recommended in Ref 12, in the case of hyperelastic materials, the uniaxial, planar and volumetric tests have been used to determine the parameters, whereas in the elastomeric foam model, the simple shear test has also been included. The Ogden, Van der Waals, and polynomial and elastomeric foam models have been evaluated, as described in the following.

The fitting parameters for the different models analyzed are shown in the succeeding tables, including the RMSE. Two expansions have been tried in the case of Ogden form, $N=1$ (Table 1) and $N=3$ (Table 2). Table 3 presents the parameters of the Van der Waals model, Table 4 of the polynomial and Table 5 of the elastomeric foam results. A comparison between the RMSE obtained makes it possible to choose between the different forms: In this case, the elastomeric foam is the most representative model, yielding a RMSE of 25.94 %. This result seems reasonable, considering that it is the only form that takes into account the compressibility of the material. As emphasized earlier, the RMSE value can be used for comparisons even though its specific value is of no relevance.

The comparison between the experimental data and the behavior of the models is represented in Figs. 19–21. Again, it can be observed that in every case and, in particular, in the case of the volumetric test, the elastomeric form is better than the rest of the models analyzed.

Summary and Conclusions

In this paper, a complete work of mechanical characterisation and analysis of behavior of a highly elastic cellular PU elastomer has been developed. This material is the main element of an elevator shock absorber.

The mechanical characterisation consists of uniaxial, planar, volumetric, and pure shear tests. In addition, several theoretical models to describe the mechanical response in hyperelastic materials and elastomeric foams have been evaluated, by fitting their corresponding parameters from the experimental information. Namely, the Ogden form (with $N=1$ and $N=3$), the Van der Waals, and the polynomial and elastomeric models have been analyzed. The small dimension specimens have been obtained from one of the buffer shock absorbers available for this work.

The numerical tools provided by the software ABAQUS have been used for the fitting process. The final results lead to the conclusion that the elastomeric foam form is the best to account for the behavior of this kind of materials. This information is of great importance because it allows the different requirements imposed by the European standards UNE-EN 81 [1–3] on the behavior of the buffer to be verified by means of finite elements simulation.

References

[1] UNE-EN 81-1: 2001, 2006, "Safety Rules for the Construction and Installation of Lifts; Part 1: Electric Lifts; A2: Machinery and pulley spaces," AENOR, Madrid.

[2] UNE-EN 81-2: 2001/A1, 2006, "Safety Rules for the Construction and Installation of Lifts-Part 2: Hydraulic Lifts," AENOR, Madrid.

[3] UNE-EN 81-3: 2001, 2001, "Safety Rules for the Construction and Installation of Lifts. Part 3: Electric and Hydraulic Service Lifts," AENOR, Madrid.

[4] ASTM, *Engineering Plastics International Handbook*, Vol. 2, ASTM International, West Conshohocken, PA, 1987.

[5] Goto, A., Yamaguchi, K., Ishiaku, U. S., and Hamada, H., "Cellular Anisotropy in Mechanical Properties of Polyurethane Foam," *Society of Plastics Engineers, Annual Technical Meeting Proceedings, SPE ANTEC*, Vol. 5, 2005, pp. 115–118.

[6] Goto, A., Yamashita, K., Nonomura, C., and Yamaguchi, K., "Modelling of Cell Structure in Polyurethane Foam," *J. Cell. Plast.*, Vol. 40, 2004, pp. 481–488.

[7] Ridha, M., and Shim, V. P. W., "Microstructure and Tensile Mechanical Properties of Anisotropic Rigid Polyurethane Foam," *Exp. Mech.*, Vol. 48, 2008, pp. 763–776.

[8] Hawkins, M. C., "Cell Morphology and Mechanical Properties of Rigid Polyurethane Foam," *J. Cell. Plast.*, Vol. 41, 2005, pp. 267–285.

[9] Ozkan, E., "Thermal and Mechanical Properties of Cellular Polystyrene Polyurethane Insulation Materials Aged on a Flat Rood in Hot Dry Climate," *J. Test. Eval.*, Vol. 22, 1994, pp. 149–160.

[10] Callister, W. D., *Materials Science and Engineering: An Introduction*, John Wiley & Sons, New York, 2006.

[11] Malvern, L. E., *Introduction to the Mechanics of a Continuous Medium*, Prentice-Hall Inc., Englewood Cliffs, NJ, 1969.

[12] Hibbit, Karlsson, Sorensen, *ABAQUS Analysis User's Manual, Version 6.5*, Vol. 3, HKS Inc., Pawtucket, RI, 2004.

[13] UNE-ISO 23529:2008, 2008, "Rubber—General Procedures for Preparing and Conditioning Test Pieces for Physical Test Methods," AENOR, Madrid.

[14] UNE 103402, 1998, "Determinación de los parámetros resistentes de una muestra de suelo en el equipo triaxial," AENOR, Madrid.